# Journal of Materials Chemistry B

Accepted Manuscript






ROYAL SOCIETY OF CHEMISTRY

www.rsc.org/materialsB

Journal Name

RSCPublishing

ARTICLE

# Study of polythiophene/water interfaces by Sum-Frequency Generation spectroscopy and Molecular Dynamics simulations

Cite this: DOI: 10.1039/xoxxoooooox

Received ooth January 2012,
Accepted ooth January 2012

DOI: 10.1039/xoxxoooooox

www.rsc.org/

S. Bellani[a,b], M. Porro[b,c], C. Caddeo[d], M. I. Saba[d], P. B. Miranda[e], A. Mattoni[d], G. Lanzani[a,b,*], M. R. Antognazza[b,*]

Semiconducting polymer/water interfaces are gaining increasing attention due to a variety of promising applications in the fields of biology and electrochemistry, such as electrochemically-gated transistors and photodetectors, that have been used for biosensing and neuroscience applications. However, a detailed characterization of the polymer surface in presence of an aqueous environment is still lacking. In this work, we employ Sum-Frequency Generation vibrational spectroscopy, a surface-specific technique compatible with electrochemical/biological conditions, to demonstrate that the surface of thin films of regio-regular poly-3-hexylthiophene (rr-P3HT) undergo a molecular reorientation when exposed to aqueous electrolytes, with respect to their surface structure in air. Experimental results are corroborated by molecular dynamics simulations. Since surface molecular orientation is believed to play a fundamental role in electrochemical and environmental stability of conjugated polymers, the reported findings not only contribute to the fundamental understanding of conjugated polymer/water interfaces, but they may also have implications to the design of conjugated polymers for enhancing their performance in electrolytic environments.

## Introduction

In recent years, research on conjugated polymers started to advance its frontiers beyond the applications in light emitting diodes, photovoltaic cells and transistors, facing new challenges in the fields of photoelectrochemistry and biology [1-8]. A plethora of novel possible applications of organic semiconductors have been reported, including photoelectrochemical cells [9-13], water-gated field effect transistors for biosensing [14-20], organic transistors for elicitation and recording of cellular activity [21-24], and photo-active interfaces with living cells and tissues [25-30]. The common denominator of all these proof-of-concept devices is the direct contact between the active polymer surface and a liquid component, which in most cases is saline water. Among all existing $\pi$-conjugated polymers, polythiophenes are by far the most employed ones, due to their distinct features: good charge carrier generation efficiency and electronic mobility, facile processability, and environmental stability. Previous work has demonstrated that polythiophene derivatives, and in particular regio-regular poly-3-hexylthiophene (rr-P3HT), preserve their optoelectronic properties, such as absorption and charge generation capability, even when in direct contact with water [31]. It has been reported that degradation processes are neither enhanced nor accelerated by interaction with aqueous saline solutions, as compared to contact with ambient oxygen [32]. Moreover, electrolyte-gated polythiophene transistors show good properties in terms of electrical performance and electrochemical or temporal stability [33].

In general, however, while it has been well established that the *bulk* optoelectronic properties of organic semiconductors are not seriously affected by the contact with water, the specific properties of the conjugated polymer/electrolyte *interface* are by far much less characterized. Nevertheless, the interface structure is believed to play fundamental roles, in many

different aspects. The interaction with the liquid, for instance, may give rise to huge local electric fields, as already reported in the case of pentacene [34]. Also, the interface capacitance established at the conjugated polymer/electrolyte interface is obviously influenced by the high dielectric constant of water. The interaction with an electrolyte may also lead to ion accumulation at the polymer surface and to doping phenomena, previously reported in the case of conducting polymers such as polyaniline and PEDOT:PSS [35-37]. For biological applications, specific adhesion proteins are often employed, which create charged nm-sized regions and may possibly change the overall interfacial behavior [38].

In particular, the molecular orientation of conjugated polymers at the interface with water plays a key role to the environmental stability and electrochemical activity [39,40]. In the case of a liquid-gated field effect transistor, for instance, the superior performance of thiophene-based devices with respect to other polymer classes was recently attributed to a specific orientation of the alkyl side chains [41]. Analogous effects may play important roles in several device configurations, including, for instance, ion-sensing field effect transistors, photoelectrochemical cells for water splitting and oxygen reduction, biological and environmental sensors, and optical or electrical bio-transducers for excitation and recording of living cells activity.

This work represents a first attempt to selectively study the interface phenomena between rr-P3HT and water, and in particular to assess if a specific molecular orientation of polymer chains is induced by the direct contact with an aqueous environment, in contrast to contact with air. One should note that the selective study of the interface with a liquid introduces severe constraints, in particular the need to work at room pressure and temperature. For this reason, many powerful surface-selective techniques, including X-ray diffraction (XRD), near-edge X-ray absorption fine structure spectroscopy (NEXAFS) and ultraviolet photoelectron spectroscopy (UPS), cannot be employed in this specific case. We thus opted for non-linear optical spectroscopy, and in particular for Sum-Frequency Generation (SFG) spectroscopy, which retains all the common advantages of optical techniques, being nondestructive and highly sensitive with good spatial, temporal, and spectral resolution, and is applicable to any interface accessible by light [42-45]. Being based on a second-order nonlinear optical process, SFG is forbidden in media with inversion symmetry, but allowed at interfaces where the inversion symmetry is necessarily broken. Consequently, SFG spectroscopy is intrinsically surface-specific for interfaces between centrosymmetric media. In particular, IR-visible SFG allows probing vibrational resonances that are generally associated with specific functional groups on the molecule [46-49].

Previous studies of non-conjugated polymers with SFG spectroscopy have demonstrated the ability of this technique to probe polymer orientation at buried interfaces, such as polymer/polymer [48,49], polymer/dielectric [50-52] or polymer/metal [53-56], and in particular surface reorientation induced by the contact with water [57-58]. For the case of organic semiconductors, their structure at semiconductor/air [59], semiconductor/metal [60-62], and semiconductor/dielectric interfaces [59, 63-64] have been investigated. In particular for P3HT, a few recent studies have addressed its reorientation at buried interfaces induced by thermal annealing [65,66] or by the surface chemistry of the substrate [64]. However, the effect of water on surface orientation of P3HT has not been addressed yet by SFG, and this is the subject of the present study.

Molecular Dynamics (MD) is a suitable theoretical tool to support SFG analysis and it has been used to study interfacial water, gas-liquid interfaces and polymer surfaces. For simple systems it is possible to directly simulate the SFG spectra through MD [67-71]. For systems with higher structural and chemical complexity (e.g. surfaces and interfaces with crystalline polymers) the direct simulation of the SFG spectra could be computationally prohibitive. Here, we make use of an alternative approach in which the atomistic simulations provide an independent theoretical estimate of the P3HT surface morphology, based on the configurational energy analysis. SFG analysis evidenced a difference in P3HT backbone orientation between polymer surfaces exposed to air or water, further confirmed by MD simulations.

## Theoretical SFG spectroscopy description

SFG is a second-order nonlinear spectroscopy in which tunable visible and IR laser sources are spatially and temporally overlapped in a sample to produce light at the sum of their frequencies: $\omega_1 + \omega_2 = \omega_3$ [42,43]. This process is forbidden in centro-symmetric media (e.g., in the bulk of most materials), but is allowed at the interfaces between dissimilar materials where the local symmetry is broken; this selection rule thus makes SFG an inherently interface-sensitive technique [42,44]. The intensity of the SFG signal generated at the interface is given by:

$$I_{SFG} \propto \left|\chi^{(2)}{}_{eff}\right|^2 I_{VIS}(\omega_1) I_{IR}(\omega_2) \quad (1)$$

where $I_{VIS}(\omega_1)$and $I_{IR}(\omega_2)$ are the intensities of the visible and IR light sources, respectively, and $\chi^{(2)}{}_{eff}$ is the effective second order susceptibility. As the IR frequency ($\omega_2$) is tuned, a vibrational spectrum of the interfacial molecules is obtained, since the generated SFG signal will vary due to vibrational enhancement of $\chi^{(2)}{}_{eff}$, which usually dominates over the non-resonant contribution from all other resonances [46-49]. For a detailed description of SFG theory, we refer the reader to the SI section. Here, we only note that the characterization of the resonant term of $\chi^{(2)}{}_{eff}$ is of particular interest, as it describes the orientational average of the hyperpolarizability of a specific molecular vibration, which is usually associated with a particular moiety of the interfacial molecules. It thus allows obtaining information about their orientation at the interface. In more detail, the resonant $\chi^{(2)}{}_{eff}$ is related to $\chi^{(2)}{}_{ijk}$, a 27-element tensor describing the nonlinear response of the



 

interface (due to three-wave mixing), which can be fully characterized by measuring the SFG spectra for all possible polarization combinations of the IR, visible and SFG beams. The selection rules for second-order processes dictate that only seven of these elements are nonzero, and, in the limit of in-plane isotropy for achiral materials, three of them are degenerate. Thus, all independent tensor elements can be determined by using four polarization combinations, where each beam may have two different polarizations, one with the electric field vector perpendicular to the plane of incidence, labeled $\hat{s}$, and another one with the electric field vector parallel to the plane of incidence, labeled $\hat{p}$. These polarization combinations are usually referred as *PPP* (with $\chi^{(2)}{}_{eff,\ PPP}$ proportional to the linear combination of the tensor elements $\chi^{(2)}{}_{xxz}$, $\chi^{(2)}{}_{xzx}$ and $\chi^{(2)}{}_{zxx}$), *SSP* ($\chi^{(2)}{}_{eff,SSP}$ proportional to $\chi^{(2)}{}_{yyz}$), *SPS* ($\chi^{(2)}{}_{eff,SPS}$ proportional to $\chi^{(2)}{}_{yzy}$) and *PSS* ($\chi^{(2)}{}_{eff,PSS}$ proportional to $\chi^{(2)}{}_{zyy}$). In the adopted convention, letters are listed in order of decreasing frequency: the first one is for the sum frequency, the second one is for the visible beam, and the last one is for the infrared beam. Therefore, with a model for the nonlinear response of a particular vibration, complete polarization-dependent characterization enables to translate the spectroscopic observables (i.e., the SFG intensity signals) into ensemble-averaged molecular orientations at interfaces. In the case of SFG from polymer thin films, spectroscopic signals can arise from multiple interfaces [72,73] and all these contributions need to be taken into account, as they interfere to yield the observed spectra.

## Materials and methods

**Polymer thin films preparation.** rr-P3HT (Sigma-Aldrich) has a regio-regularity of 99.5% and an average molecular weight of $54{,}000 - 75{,}000\ g/mol$; it has been used without any further purification. As thorough cleaning of the $CaF_2$ substrates was required, rinses were sequentially performed in an ultrasonic bath with the following cleaning solutions: a specific tension-active agent in a water solution (HELLMANEX® II, 3 %), deionized water, pure acetone and isopropyl alcohol. Chlorobenzene solutions of rr-P3HT were prepared in a concentration of $35\ g/l$ and $5 g/l$, subsequently heated to $50\ °C$ for $20\ min$, stirred and finally deposited onto previously heated substrates by spin-coating. The spinning parameters (angular acceleration $1200\ rad/s^2$ for $35\ g/l$ solution and $1200\ rad/s^2$ for $5\ g/l$ solution; deposition duration $60\ s$) were carefully selected to obtain suitable optical quality and film thickness ($\sim 300\ nm$ and $10\ nm$, as deduced by profile measurement (KLA TENCOR, Alpha Step 500)). After deposition, organic layers were annealed for $20\ min$ at $140\ °C$, in order to evaporate residual solvent in the polymer films. The preparation of the solution and the deposition of the P3HT film were performed in air, while the annealing process was performed under inert atmosphere.

**IR-Visible SFG Spectroscopy.** In the IR-Visible SFG experiment, we used a commercial SFG spectrometer from EKSPLA (Lithuania). Briefly, it is based on an active-passive mode-locked Nd:yttrium aluminum garnet (YAG) laser (EKSPLA, model PL 2143A20) at 1064 *nm* with 30 *ps* pulse width, 30 *mJ* pulse energy and 20 *Hz* repetition rate. Its frequency-doubled output at 532 *nm* was used as the visible input ($\omega_1$, resonant with the rr-P3HT absorption). The tunable IR beam ($\omega_2$) was generated in a $AgGaS_2$ crystal by difference frequency mixing of the fundamental of the Nd:YAG laser with the output of an optical parametric generator/amplifier system (EKSPLA, model PG401/DFG2-10P) pumped by the third harmonic of the laser (355 *nm*). The visible and IR beams were spatially and temporally overlapped at the surface of the sample with incidence angles of 61° and 55°, respectively, leading to the generation of the SFG signal. Each beam had its polarization set to *S* or *P* by polarizers (visible or SFG beams) or mirror sets (for the IR beam). The beam sizes were approximately $1.2\ mm$, while the pulse energy were $20\ \mu J$ and $30\ \mu J$, for the visible and infrared beams, respectively. The intensity of the visible beam, in particular, was properly adjusted to that value in order to avoid optical damage to the sample, which results from the high peak intensities of both beams. However, due to the low repetition rate of the laser, the average power on the sample (and therefore its average heating) is quite low, less than 1 mW. The SFG output in the reflected direction (reflected angle 60°) was detected by a photomultiplier with gated electronics after proper spatial and spectral filtering. Under these conditions, the SFG spectra were obtained for the three polarization combinations (*SSP*, *PPP*, *SPS*) on the same point of the sample. To correct the spectra for the response of the detection system, OPA/DFG performance, water vapor absorption and changes in overlap of visible and IR beams, they were normalized by the nonresonant SFG spectrum of a ZnS thin film on glass. The sample was placed on a thoroughly cleaned Teflon cell with the polymer film facing down, and the beams coming from the top side ($CaF_2$ substrate). After measurement of SFG spectra with the film exposed to air, the cell was filled with ultrapure water (Milli-Q, resistivity 18.3 MΩ·cm) and SFG spectra were acquired on the same spot of the sample, but with the rr-P3HT film now in contact with water. In order to avoid the strong IR absorption from water, incidence direction of the beams was from the $CaF_2$ substrate side.

**Molecular Dynamics Simulations.**

MD can be employed to elucidate the conformation of the systems either through SFG simulation [67-71] or by energetic analyses [74,75]. In order to simulate the SFG spectra it is required to know (i) the molecular polarizability (which must be obtained from computationally demanding ab initio calculations, and can be different for different molecular groups or even for the same molecular group in a different chemical environment), (ii) the concentration of the molecular groups (thiophene rings, alkyl chains) at the surface and (iii) their orientation distribution (its average and width). Accordingly,

the simulation of the SFG for systems with a complex free energy landscape is challenging and it is not performed for the present case of P3HT crystals formed by finite chains.

At room temperature the polymer surface has a large number of local minima separated by large free energy barriers and the system can be blocked in metastable configurations. An effective strategy is to simulate the system at different ($\vartheta$, $\gamma$) and to calculate the corresponding energy in order to find the minimum (i.e. most probable) configurations.

To this aim we followed a two-steps procedure: we have employed finite temperature MD to generate the reference atomistic models of bulk polymer and water while we have used a quasistatic approach at T ~ 0 K (i.e. local optimization) to calculate the energies of the P3HT/water and P3HT/vacuum systems at the different ($\vartheta$, $\gamma$) pairs.

More in detail, a series of P3HT slabs of the same width and different crystallographic orientations ($\vartheta$, $\gamma$) was generated, each formed by 60 finite chains terminated with a methyl group. In order to keep the computational workload affordable we restricted our analysis to the two extreme values of $\gamma$, namely 0° (face-on) and 90° (edge-on). Starting from a vertical ($\vartheta$ = 0°) configuration, the chains were then tilted by different angles, ranging from 10° to 80°. The vertical configuration is a special case in which the face-on and edge-on configurations are identical. The polymer-water interface was obtained by covering the P3HT layer by a film of liquid water. The systems consist of 105 atoms on average, with the biggest one containing 71410 water molecules. The VMD 1.9 [76] package was used to build the P3HT-water systems. Figure 1 shows two examples of starting configuration for $\gamma$ = 0° (left panel, $\vartheta$ = 30° in vacuo) and $\gamma$ = 90° (right panel, $\vartheta$ = 60° in water). In order to avoid size effects due to the periodic boundary conditions and interactions between replicas, we put special care in keeping it constant the width of the polymer slab: to this aim, the length of polymer chains was consistently increased with the tilt angle. More details on the simulation protocol are provided in the Supporting Information.

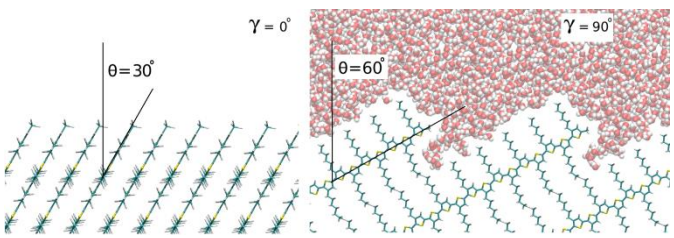


Figure 1. Examples of starting configurations systems for $\gamma = 0°$ (left panel, $\theta = 30°$ in vacuo) and $\gamma = 90°$ (right panel, $\theta = 60°$ in water) .

As for the force field, the P3HT polymer and the water layer have been modeled using the General Amber Force Field (GAFF) [77-79], which has been successfully applied to study conjugated polymers, in particular poly(3-alkylthiophenes) [80-82]. The atomic partial charges of the polymer were calculated according to the standard AM1-BCC method [83]. We have used the TIP3P model for water (which includes the charges) [84]. The dispersive (i.e. Van der Waals) interactions (both intra- and intermolecular) are described by the sum of two-body Lennard-Jones contributions, with Amber force field parameters. Model potential molecular dynamics simulations were performed with the NAMD molecular simulations package (v. 2.9) [85] with the rigid bond constraint for the hydrogens. The equations of motion of atoms were integrated by using the Velocity Verlet algorithm with a time step as small as 1 fs. Multiple time stepping was used, with short-range nonbonded interactions calculated every two time steps and full electrostatics evaluated every time step. Periodic boundary conditions (PBC) in all directions were always used. All the electrostatic contributions were computed by the Particle Mesh Ewald (PME) sum method, with PME grid spacing of 1 Å. Temperature was controlled by Langevin thermostat with damping coefficient $\nu = 1\ ps^{-1}$.

## Results and discussion

### SFG spectroscopy

Thin films of rr-P3HT spin coated on $CaF_2$ substrates were studied via SFG spectroscopy at the interface with ambient air and ultrapure water. A sketch of the experimental set-up is shown in Figure 2.

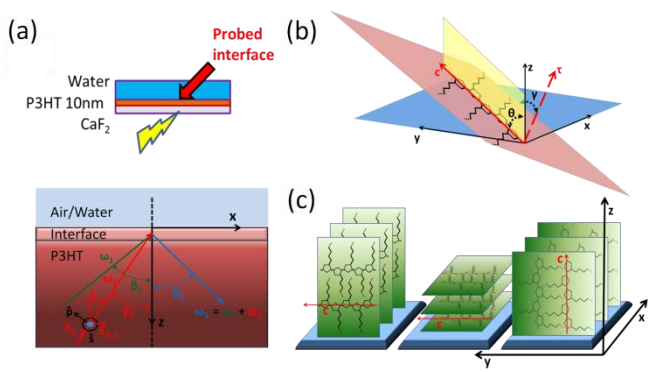


Figure 2. (a) Sketch of the considered interface and of the set-up geometry; (b) definition of lab (*xyz*) and molecular (*abc*) coordinates; the chain tilt angle θ, defined as the angle between the axes *c* and *z*, and the twist angle γ, defined as the angle formed between the torsion versor τ and the vertical plane *cz*, are also shown; (c) sketch of prototypical molecular arrangement of rr-P3HT; *c* indicates the orientation axis of the polymer chain. From left to right: *edge-on*, *face-on* and *vertical* configurations.

Panel (a) shows the considered interface as probed by SFG spectroscopy. $(x, y, z)$ are the lab Cartesian coordinates; the orientation of the polarization versors $\hat{s}$ and $\hat{p}$ are also shown. In panel (b) the laboratory reference system of panel (a) is represented, together with a representative example of a possible molecular orientation with respect to the lab coordinates. $c$ denotes the axis of the molecular backbone, while $\tau$ is defined as a torsion versor, perpendicular to the median plane of two consecutive monomers, forming an angle $\gamma$ (chain twist angle) with the vertical plane defined by the axes $z$ and $c$ (shaded yellow area in Figure 2b).

From the specific molecular symmetry properties of P3HT [86] (see Supporting Information Section for more details), it is

possible to specify its molecular orientation respect to the laboratory coordinates by using only two angular coordinates, namely $\gamma$ and $\theta$. $\theta$ (chain tilt angle) defines the angle between axes $c$ and $z$ (i.e., $\theta = 0°$ indicates the direction of the polymeric chain perpendicular to the interface, while $\theta = 90°$ represents the polymer backbone parallel to the interface). $\gamma = 0°$ and $\gamma = 90°$ indicate the average plane of thiophene rings, parallel and perpendicular to the interface, respectively. Limiting configuration cases are shown in Figure 2 (panel c) and can be summarized as:

(i) $\theta \sim 90°$ and $\gamma \sim 90°$: alkyl chains are perpendicular to the interface ('edge-on' configuration, with $\pi$-stacking along the interface);

(ii) $\theta \sim 90°$ and $\gamma \sim 0°$ : the thiophene rings lye on the same plane of the surface ($\pi$-stacking perpendicular to the interface, 'face-on' configuration).

(iii) $\theta \sim 0°$ and $0° < \gamma < 90°$: thiophene backbone and alkyl side chains perpendicular and parallel, respectively, to the interface plane ('vertical' or 'end-on' configuration)

Many different studies [66, 87-96] have investigated preferential molecular orientation of rr-P3HT thin films in contact with air, highlighting the important role of several processing parameters, including spin coating solvent and speed, annealing time and temperature, regio-regularity and molecular weight. While the polymer bulk appears to be a mixture of different possible orientations [66,87], many authors have highlighted a preferential 'edge-on' orientation at the interface with air [89-93]. It is worth emphasizing that in most of these works a 'vertical' configuration was *a priori* ruled out, assuming the backbone axis *c* parallel to the surface. However, some recent reports highlighted how the overall molecular orientation is dictated by a trade-off between the interaction of the opposite medium with both the polymer alkyl side chains and the backbone end groups notably yielding a vertical orientation at the surface exposed to air [97,98].

Figure 3 shows the SFG spectra obtained in the spectral region between $1300 - 1550\ cm^{-1}$ with the three independent non-vanishing polarization combinations *PPP*, *SPS* and *SSP*, for a thin film (~ 10 nm) of rr-P3HT spin coated on $CaF_2$ and in contact with air (panel a, open symbols) and water (panel b, open symbols). The agreement between experimental results and fitting curves (represented as solid lines) obtained by superposing several vibrational resonances of the P3HT backbone (see SI section, eq. S14) is satisfactory.

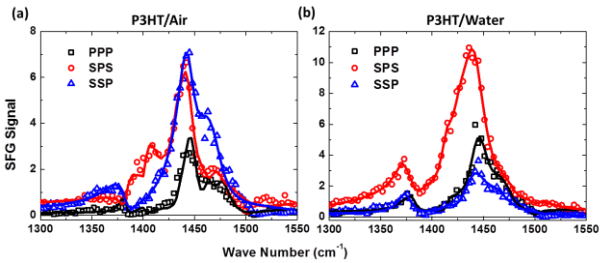


Figure 3. SFG spectra measured for a thin film of rr-P3HT in contact with air ((a), open symbols) and with water ((b), open symbols) for three different polarization sets. Results of the fitting to a superposition of vibrational resonances of the P3HT backbone are represented, for each polarization set, as solid lines.

In agreement with results reported in literature for rr-P3HT thin films [62-65] SFG spectra are dominated by C-C intra-ring stretch ($\sim 1380\ cm^{-1}$) and C=C symmetric stretch ($\sim 1440\ cm^{-1}$) modes. First of all, we note that there are no significant differences in the vibrational frequencies in the case of direct exposure to the water environment as compared to exposure to open air, supporting the fact that the contact with water does not significantly affect the conjugation properties of the polymer, and does not lead to a specific enhancement of the irreversible degradation processes. Similar conclusions were previously reported for rr-P3HT exposed to ultrapure water, based on detailed Raman and IR analysis [32]. Noteworthy, the ratio between the maximum intensity (at $\sim 1440\ cm^{-1}$) for *PPP* and *SPS* polarization combinations is similar in the two cases; conversely, the *SSP* component shows a ~ 60% decrease in intensity for the interface with water as compared to the interface with ambient air. This evidence represents a first indication that the orientation of the thiophene rings at the two interfaces might be different. To calculate the absolute orientation of the P3HT backbone in the two cases, we employ a suitable model for the non linear polarizability of the P3HT molecule (see SI for more details) [62]. As briefly stated above and described in the SI section, by exploiting the specific molecular symmetry properties of P3HT it is possible to specify its molecular orientation with respect to the lab coordinates simply by two angular coordinates $\theta$ and $\gamma$ (Figure 2b). Figure S4 shows the calculated $\chi_{C=C}^{(2)}$ components based on the adopted rr-P3HT molecular model for C=C symmetric stretch, and for the three considered polarization combinations. Comparing the $\chi_{C=C}^{(2)}$ tensor components obtained from the fitting of the SFG spectra with those obtained by the theoretical angular function for $\chi_{C=C_{eff}}^{(2)}$ it is possible to provide an estimate of the admissible range for the pair of angles $(\theta, \gamma)$, i.e., a hint of the most probable molecular orientation at the interface.

Figure 4 displays $(\theta, \gamma)$ plots of $\Delta_r$, a measure of the discrepancy between the experimental values of the $\chi_{C=C}^{(2)}$ components and the ones expected from the theoretical model for a given polymer backbone orientation $(\theta, \gamma)$, in units of standard deviation of the experimental values. Admissible regions are thus identified by values close to zero (red-orange), while forbidden regions are represented in green-blue colors.

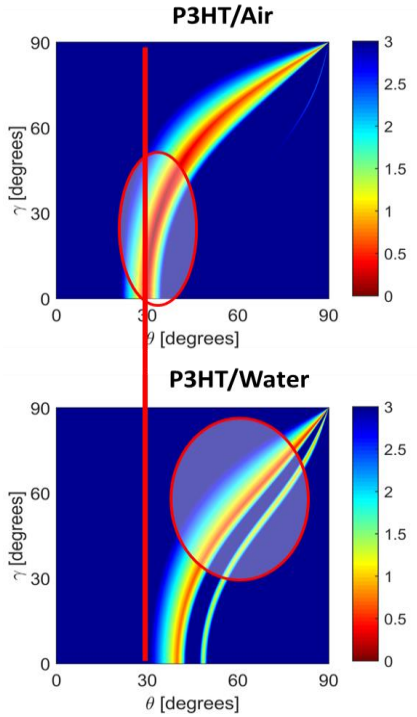


Figure 4. $(\theta,\gamma)$ plots of $\Delta_r$, a measure of the discrepancy between the experimental and theoretical values of the $\chi_{C=C}{}^{(2)}$ components for a given chain orientation. The red ellipses highlight the most favored orientation of the rr-P3HT conjugated backbone at the interface with air (top panel) and with water (bottom panel). The color bar is in units of standard deviation between experimental values and theoretical ones; most favored orientation thus corresponds to $(\theta,\gamma)$ values in red/orange regions.

It clearly emerges that the direct contact with water excludes the most probable values obtained in the case of exposure to air, and promotes instead a slightly different molecular arrangement, as far as the polymer surface is concerned. In particular, at the air interface $\theta$ preferentially assumes values near $30°-40°$, while $\gamma$ increases from 0° to 50° for $\theta$ approaching the maximum value of 40°. This indicates a preferential (tilted) 'end-on' type arrangement. Conversely, the interface with water only admits $\theta > 40°$, with $\gamma$ increasing from 0° to 90° for $\theta \to 90°$, thus indicating a change with respect to the previous case. In general, these data suggest an overall relaxation of the vertical configuration, with a more pronounced parallel orientation of the backbone respect to the interface. Incidentally, we note that the limit $\theta = \gamma = 90°$ cannot be detected by SFG, because it represents an isotropic arrangement. Thus, a distribution of $\theta > 40°$ values with the appropriately increasing $\gamma$ (towards 90°) would be also consistent with the experimental spectra. This means that the P3HT chains in contact with water tend to become more aligned along the interface, but with a more edge-on (instead of face-on) orientation.

Importantly, we note that the contribution of the substrate/P3HT interface had to be taken into account in our analysis, since we employed very thin films with light incident from the substrate side (in order to avoid strong absorption of the IR beam by water). We thus carried out a complete analysis also in the case of a thick polymer sample (approximately 300 $nm$), from which we could determine the contribution from the substrate/P3HT interface, since in this case it overwhelms the contribution from the P3HT/water(air) interface (see Supplementary Figure S5). For the sake of completeness, we also considered the experimental geometry with light incidence from the opposite direction (i.e., from the air side, onto the polymer surface), for thick polymer films exposed to air. Analogous results were obtained in this case with respect to the thin film, further confirming the predominance of a near vertical arrangement dictated by the specific contact with air (see Supplementary Figure S6).

As a further step of our investigation, we also considered if the presence of salts in solution had considerable effects on molecular orientation at polymer/solution interface. Figure 5 shows the SFG spectra obtained after adding sodium chloride (NaCl 0.1 $M$ concentration) to ultrapure water, at the three considered polarization combinations. In each case, the lack of significant differences, with respect to ultrapure water suggests that the presence of the salt, at concentrations of the same order of typical biological environment, does not considerably alter the morphological structure and molecular orientation of the rr-P3HT polymer surface.

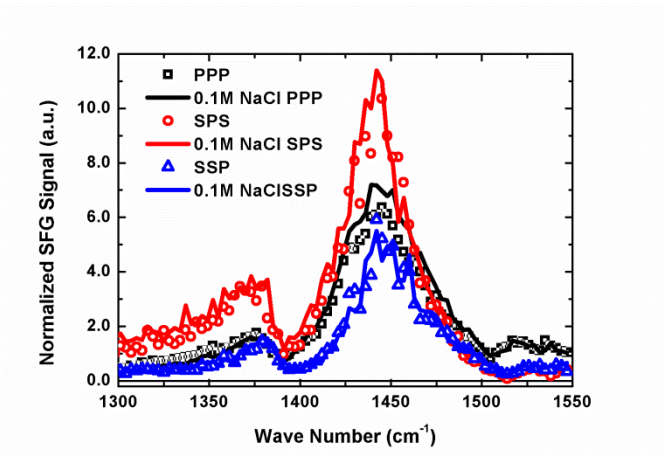


Figure 5. Experimental SFG spectra with three polarization sets for a thin film of rr-P3HT in contact with ultrapure water (open symbols) or with aqueous saline solutions of biological relevance (NaCl 0.1 $M$, solid lines).

### Molecular dynamics simulation

Preferential molecular orientation of rr-P3HT at interface with water, as derived by SFG spectroscopy, is further confirmed by molecular dynamics simulations.

By comparing the energy of each system to the corresponding bulk phases (see Supporting Information) it was possible to calculate the formation energy in vacuo $\sigma_P(\gamma,\theta)$ and in water $\sigma_{P/w}(\gamma,\theta)$ as a function of the backbone angle $\theta$ for the two orientations $\gamma = 0°$ and $\gamma = 90°$. The most stable configurations are those with the lowest formation energy.

In Fig. 6 we report the atomistic data in vacuo (top panels) and in water (bottom panels) for $\gamma = 0°$ (red) and $\gamma = 90°$ (green).

The zero of the energy scale is set to the energy of the vertical polymer ($\theta = 0°$).

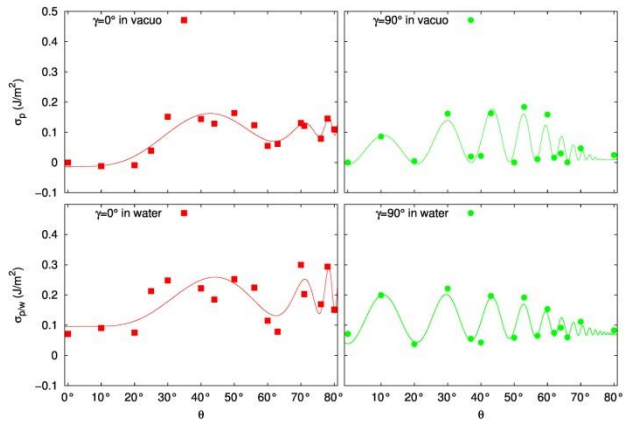


Figure 6. Surface energy for different $\theta$ angles in vacuo (top) and in water (bottom). Filled squares and circles are the atomistic values and lines are fitting functions.

The main results are: (i) the energy depends sizably on the tilt angles with oscillations that can be attributed to the molecular staggering; it is found that there is a large number of local minima in which the polymer can be locally stable; (ii) on average, the presence of water increases the formation energy of the polymer by about $0.1\,J/m^2$, consistently with the polymer hydrophobicity.

In order to understand the oscillating behavior and to compare the relative stability of the different polymer orientations we developed an analytical model to fit the atomistic data. The model takes into account two contributions: (i) an oscillating energy cost due to the intermolecular staggering $\sigma_1(\theta)$; (ii) a term related to the amount of polymer exposed to the surface that depends on the tilt, $\sigma_2(\theta)$. In order to explain the above terms we sketched the polymer interface for a given $\theta$ (see Supplementary Figure S7).

Let's focus on the edge-on configuration first (e.g. Figure 6, right panel). When $\theta = 0°$ (vertical configuration), the P3HT chains are perfectly aligned and interdigitated and the intrachain energy has a minimum. When the chains are tilted by an angle $\theta$, instead, there is a chain shift along the backbone direction equal to $x = d * tg(\theta)$ (see Supplementary Figure S7). The shift increases monotonically with the angle while the intrachain energy oscillates between the staggered and the aligned energy [80]. The period $b$ of the oscillation must correspond to the periodicity along the backbone (7.75 Å [99]). Accordingly, the staggering energy can be written as:

$$\sigma_1(\theta) = \delta(\theta)\left[1 - cos\left(\frac{x}{b}2\pi\right)\right] \quad (2)$$

where $\delta(\theta)$ is the staggering energy amplitude which depends on $\theta$.

The same analysis holds also for the face-on orientation, once $d$ is set to the corresponding value (the distance $d$ is 20 Å for the edge-on and 4 Å for the face-on).

The second term $\sigma_2(\theta)$ of the model is introduced to describe the interaction of the polymer at the interface. Let's consider first the case $\gamma = 0°$. For $\theta = 0°$ the surface energy $\Gamma_v$ is that of the polymer cut of the vertical configuration along the (001) plane; for $\theta = 90°$ it corresponds to the surface energy $\Gamma_h$ of the horizontal cut that is (010) or (100) for $\gamma = 0°$ or $\gamma = 90°$, respectively). For intermediate values $0° < \theta < 90°$, the polymer-surface interaction is calculated as an average between the two values. The proportion between the two is illustrated in Supplementary Figure S7: the blue segment corresponds to the $\Gamma_v$ vertical contribution and the red one to the $\Gamma_h$ horizontal part. This corresponds to the function:

$$\sigma_2(\theta) = \Gamma_v cos^2(\theta) + \Gamma_h sin^2(\theta) \quad (3)$$

In conclusion, by summing the two terms we get the model for the energy dependence on $\theta$:

$$\sigma(\theta) = \delta(\theta)\left[1 - cos\left(2\pi\frac{d}{b}tg(\theta)\right)\right] + \Gamma_v cos^2(\theta) + \Gamma_h sin^2(\theta) \quad (4)$$

Where the staggering energy amplitude $\delta(\theta)$ is fitted against atomistic data together with $\Gamma_v$ and $\Gamma_h$. The results show that the model is able to reproduce the oscillating behavior with the expected periods $(b/d)tg^{-1}(\theta)$ so clearly attributing the oscillation to the staggering effect.

In order to analyze the calculated formation energies in vacuo and in water and to better compare the optimized atomistic configurations with the results of experiments (performed at room temperature) we locally averaged the oscillating term in the model. This was equivalent to remove the cosine behavior and to retain only the $\delta(\theta)$ in the first term of the model. The averaged curves are reported in Figure 7 for the case of vacuum (left) and water (right).

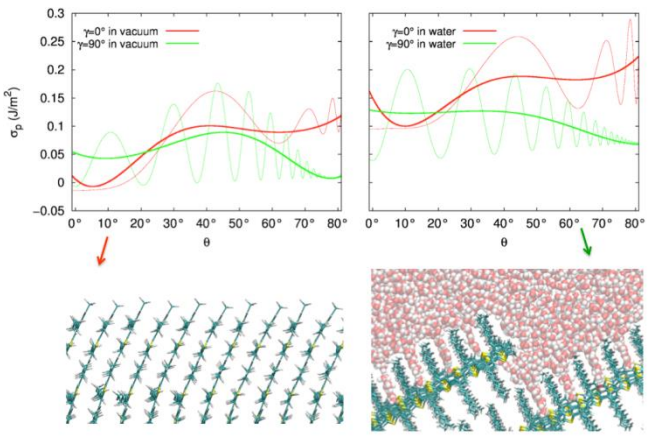


Figure 7. (Top panels) Averaged formation energy for P3HT surface in vacuo (left) and in water (right). (Bottom panels) Atomistic configurations corresponding to the minimum energy.

The upshift of the curves due to water and the hydrophobicity is now more evident (compare right and left panel). In vacuo (left

panel) the absolute minimum occurs for vertical face-on (red) configurations with the face-on curve crossing the edge-on one (green) at around $\theta = 30°$. In water, the lowest energy configurations are found at $\theta > 40°$. The different molecular orientations predicted by the atomistic simulations are in qualitative good agreement with the reported SFG results highlighting more vertical orientations in air and more horizontal edge-on configurations in water.

One should notice that some important differences still exist between theory and experiments. Experiments give a smaller range of possible $\theta$ values while the atomistic simulations (even after averaging) indicate possible secondary configurations. For example, the local minimum in vacuo corresponding to possible face-on horizontal configurations has not any correspondence in the experimental data. This difference can be attributed to a kinetic barrier preventing the system to explore such configurations by starting from the minimum or to several physical factors that are not included within the model: thermal effects, termination of the polymer chains by different chemical groups, chemical contaminations possibly occurring both in air and in water, coexistence of different molecular orientations within the surface, trapping of the system into local minimum energy configurations, and so on. Nevertheless, the simulations provide a clear theoretical evidence that the vertical configuration in air is not only possible but likely energetically favorable. Furthermore, the calculations support the observed tendency of the polymer towards a horizontal configuration in water with a preference for exposing the alkyl chains in an edge-on configuration.

## Conclusions

In this work we employed surface-specific SFG spectroscopy to selectively study the molecular orientation of a rr-P3HT thin film exposed to direct contact with water, and we compared our results with the case of open air exposure. The peculiar molecular alignment at the polymer surface, dictated by the presence of an aqueous environment, beyond its interest as a fundamental study, can have important consequences in practical applications, since it is expected to play a role in all electrical and chemical processes occurring at the interface. Experimental results put in evidence that the direct contact with water actually promotes a different molecular arrangement, as far as the polymer surface is concerned, with a preferential 'edge-on' configuration in the case of water and a 'vertical' one in the case of open air. This implies a more pronounced parallel orientation of the backbone respect to the water interface. Experimental results were confirmed by molecular dynamics simulations. In particular, the specific alignment of the side alkyl chains, perpendicular to the polymer/water interface, could act as a physical barrier between the polymer backbone and the electrolytic environment. On one side, this may justify the remarkably good electrochemical stability, as widely reported for thiophene-based polymers, at the base of many biomedical applications. On the other side, it can certainly represent a limitation to the charge transfer efficiency, thus explaining the low efficiency of photoelectrochemical cells based on bare conjugated polymers.

Overall, our results represent an extension of previous SFG studies of environmental effects on polymer interfaces to the case of conjugated polymer/aqueous electrolyte interfaces. They may have implications to the understanding and engineering of conjugated polymer interfaces for electrochemical and biological applications.

## Acknowledgements

The work was supported by EU through projects FP7-PEOPLE-212-ITN 316832-OLIMPIA, the Future and Emerging Technologies (FET) programme under the FP7, Collaborative Project 309223 (PHOCS), Istituto Italiano di Tecnologia (IIT) under "Platform Computation", Regione Autonoma della Sardegna under L.R. 7/2007 CRP-24978 and CRP-18013. Support from Telethon – Italy (grants GGP12033 and GGP14022), and Fondazione Cariplo (grant ID 2013-0738) is also acknowledged. Computational support has been provided by CINECA through ISCRA Projects TIPTAP and SOAP.

## Notes and references

[a] Politecnico di Milano, Dip.to di Fisica, P.zza L. da Vinci 32, 20133 Milano, Italy.
[b] Center for Nano Science and Technology @PoliMi, Istituto Italiano di Tecnologia, Via Pascoli 70/3, 20133 Milano, Italy.
[c] Politecnico di Milano, Dip.to di Matematica, P.zza L. da Vinci 32, 20133 Milano, Italy.
[d] Istituto Officina dei Materiali CNR-IOM SLACS Cagliari, Cittadella Universitaria 09042, Monserrato (CA), Italy.
[e] Instituto de Fisica de Sao Carlos, Universidade de Sao Paulo, CP 369, Sao Carlos (SP), 13560-970, Brazil.

Electronic Supplementary Information (ESI) available: Sum-Frequency Generation theory and P3HT molecular modelling; analysis of thick samples; surface energy calculation from molecular dynamics simulations; Supplementary Figures S1-S7. See DOI: 10.1039/b000000x/

1. Köhler, H. Bässler, Electronic Processes in Organic Semiconductors, 2015, J. Wiley&Sons, ISBN: 978-3-527-33292-2.
2. Organic Electronics: Emerging concepts and Technologies, 2013, ed. By F. Cicoira and C. Santato, J. Wiley&Sons, ISBN: 978-3-527-65098-9.



 

3. Organic semiconductors in sensors applications, ed. by D. A. Bernards, G. Malliaras, R. Owens, Springer Verlag ed., Berlin, 2008.
4. P. Fattahi, G. Yang, G. Kim, M. R. Abidian, Adv. Mater., 2014, 26, 1846.
5. J. Rivnay , R. M. Owens , and G. G. Malliaras, Chem. Mater., 2014, 26, 679.
6. M. Muskovich, C. J. Bettinger, Adv. Healthcare Mater., 2012, 1, 248.
7. G. Suppes, E. Ballard, S. Holdcroft, Polymer Chemistry, 2013, 4, 5345.
8. B. Winther-Jensen, D.R. MacFarlane, En. Environ. Sci., 2011, 4, 2790.
9. E. Lanzarini, M. R. Antognazza, M. Biso, A. Ansaldo, L. Laudato, P. Bruno, P. Metrangolo , G. Resnati , D. Ricci , G. Lanzani, J. Phys. Chem. C, 2012, 116, 10944.
10. T. Bourgeteau, D. Tondelier, B. Geffroy, R. Brisse, C. Laberty-Robert, S. Campidelli, R. de Bettignies, V. Artero, S. Palacina, B. Jousselme, En. Environ. Sci. 2013, 6, 2706.
11. A. Guerrero, M. Haro, S. Bellani, M. R. Antognazza, L. Meda, S. Gimenez, J. Bisquert, En. Environ. Sci., 2014, 7, 3666.
12. V. G. Khomenko, V. Z. Barsukov, A. S. Katashinskii, Electrochimica Acta, 2005, 50, 1675.
13. K. Lee, L. Zhang, H. Lui, R. Hui, Z. Shi, J. Zhang, Electrochimica Acta, 2009, 54, 4704.
14. L. Kergoat, L. Herlogsson, D. Braga, B. Piro, M.-C. Pham, X. Crispin, M. Berggren, G. Horowitz, Adv. Mater., 2010, 22, 2565.
15. M. Y. Mulla, E. Tuccori, M. Magliulo, G. Lattanzi, G. Palazzo, K. Persaud, L. Torsi, Nature Commun. 2015, DOI: 10.1038/ncomms7010.
16. C. Suspene, B. Piro, S. Reisberg, M.-C. Pham, H. Toss, M. Berggren, A. Yassar, and G. Horowitz, J. Mater. Chem. B, 2013, 1, 2090.
17. M. Magliulo, A. Mallardi, M. Yusuf Mulla, S. Cotrone, B. R. Pistillo, P. Favia, I. Vikholm-Lundin, G. Palazzo, L. Torsi, Adv. Mater., 2013, 25, 2090.
18. T. Cramer, A. Campana, F. Leonardi, S. Casalini, A. Kyndiah, Murgia, F. Biscarini, J. Mater. Chem. B, 2013, 1, 3728.
19. F. Buth, D. Kumar, M. Stutzmann, J.A. Garrido, Appl. Phys. Lett., 2011, 98, 153302.
20. H. Toss, C. Suspène, B. Piro, A. Yassar, X. Crispin, L. Kergoat, M.-C. Pham, M. Berggren, Org. Electron., 2014, 15, 2420.
21. V. Benfenati, S. Toffanin, S. Bonetti, G. Turatti, A. Pistone,M. Chiappalone, A. Sagnella, A. Stefani, G. Generali, G. Ruani, D. Saguatti, R. Zamboni M. Muccini, Nat. Mater, 2013, 12, 672.
22. D. Khodagholy, T. Doublet, P. Quilichini, M. Gurfinkel, P. Leleux, A. Ghestem, E. Ismailova, T. Hervé, S. Sanaur, C. Bernard, G. G. Malliaras, Nature Commun., 2013, 4, 1575.
23. D. Khodagholy, J. N. Gelinas, T. Thesen, W. Doyle, O. Devinsky, G. G. Malliaras, G. Buzsáki, Nature Neurosci., 2015, 18, 310.
24. A. Campana, T. Cramer, D.T. Simon, M. Berggren, F. Biscarini, Adv. Mater. 2014, 26, 3874.
25. D. Ghezzi, M. R. Antognazza, R. Maccarone, S. Bellani, E. Lanzarini, N. Martino, M. Mete, G. Pertile, S. Bisti, G. Lanzani, F. Benfenati, Nature Photon., 2013, 7, 400.
26. V. Benfenati, N. Martino, M. R. Antognazza, A. Pistone, S. Toffanin, S. Ferroni, G. Lanzani, M. Muccini, Adv. Healthcare Mater., 2014, 3, 306.
27. D. Ghezzi, M. R. Antognazza, M. Dal Maschio, E. Lanzarini, F. Benfenati, G. Lanzani, Nature Commun., 2011, 2, 166.
28. V. Gautam, D. Rand, Y. Hanein, K. S. Narayan, Adv. Mater., 2014, 26, 17512.
29. M. R. Antognazza, N. Martino, D. Ghezzi, P. Feyen, E. Colombo, D. Endeman, F. Benfenati, G. Lanzani, Adv. Mater. 2014, DOI: 10.1002/adma.201403513.
30. N. Martino, P. Feyen, M. Porro, C. Bossio, E. Zucchetti, D. Ghezzi, F. Benfenati, G. Lanzani, M. R. Antognazza, Sci. Rep. 2015, 5, 8911.
31. M. R. Antognazza, D. Ghezzi, D. Musitelli, M. Garbugli, G. Lanzani, Appl. Phys. Lett., 2009, 94, 243501.
32. S. Bellani, D. Fazzi, P. Bruno, E. Giussani, E. Canesi, G. Lanzani, and M. R. Antognazza, J. Phys. Chem. C, 2014, 118, 6291.
33. R. Porrazzo, S. Bellani, A. Luzio, C. Bertarelli, G. Lanzani, M. Caironi, M. R. Antognazza, APL Materials, 2014, 3, 014905.
34. T. Cramer, T. Steinbrecher, T. Koslowski, D. A. Case, F. Biscarini, F. Zerbetto, Phys. Rev. B, 2009, 79, 155316.
35. X. Wang, B. Shapiro, E. Smela, Adv. Mater., 2004, 16, 1605.
36. A. Lisowska-Oleksiak , A. Kupniewska, Solid State Ionics, 2003, 157, 241.
37. E. Stavrinidou, P. Leleux, H. Rajaona, D. Khodaghol, J. Rivnay, M. Lindau, S. Sanaur, G. G. Malliaras, Adv. Mater., 2013, 25, 4488.
38. S. S. Rao, J. O. Winter, Frontiers in Neuroengineering, 2009, 2, 1.
39. J. J. Lopez Cascales, A. J. Fernandez, T. F. Otero, J. Phys. Chem. B, 2003, 107, 9339.
40. D. A. Morton-Blake , D. Leith, J. Molecul. Liquids, 2009, 144, 75.
41. R. Porrazzo, S. Bellani, A. Luzio, E. Lanzarini, M. Caironi, M. R. Antognazza, Org. Electron., 2014, 15, 2126.
42. Y. R. Shen, J. Phys. Chem. C, 2012, 116, 15505.
43. A. G. Lambert, P. B. Davies, D. J. Neivandt, Appl. Spectr. Rev., 2005, 40, 103.
44. F. Vidal, A. Tadjeddine, Rep. Progr. Phys., 2005, 68, 1095.
45. H. F. Wang, L. Velarde, W.Gan, L. Fu, Annual Rev. Phys. Chem., 2015, 66, 189.
46. Y. R. Shen, V. Ostroverkhov, Chem. Rev., 2006, 106, 1140.
47. X. Lu, S. A. Spanninga, C. B. Kristalyn, Z. Chen, Langmuir, 2010, 26, 14231.
48. C. Chen, J. Wang, M. A. Even, Z. Chen, Macromolecules, 2002, 35, 8093.
49. X. Zuang, P. B. Miranda, D. Kim, Y. R. Shen, Phys. Rev. B, 1999, 59, 12632.
50. Z. Chen, Polymer International, 2007, 56, 577.
51. C. Zhang, J. N. Myers, Z. Chen, Soft Matter, 2013, 9, 4738.
52. A. Opdahl, T. S. Koffas, E. Amitay-Sadovsky, J. Kim, G. A. Somorjai, J. Phys. Cond. Matt., 2004, 16, R659.

53. I. Yagi, K. Inokuma, K. Kimijima, H. Notsu, J. Phys. Chem. C, 2014, 118, 26182.
54. X. Lu, D. Li, C. B. Kristalyn, J. Han, N. Shephard, S. Rhodes, G. Xue, Z. Chen, Macromolecules, 2009, 42, 9052.
55. X. Lu, B. Li, P. Zhu G. Xue, D. Li, Soft Matter, 2014, 10, 5390.
56. X. Lu, J. N. Myers, Z. Chen, Langmuir, 2014, 30, 9418.
57. K. Uosaki, H. Noguchi, R. Yamamoto, S. Nihonyanagi, J. Am. Chem. Soc., 2010, 132, 17271.
58. Z. Chen, Progr. Polym. Sci., 2010, 35, 1376.
59. Q. Li, R. Hua, K. C. Chou, J. Phys. Chem. B, 2008, 112, 2315.
60. T. Miyamae, K. Tsukagoshi, W. Mizutani, Phys. Chem. Chem. Phys., 2010, 12, 14666.
61. T. Miyamae, E. Ito, Y. Noguchi, H. Ishii, J. Phys. Chem. C, 2011, 115, 9551.
62. F. C. B. Maia, P. B. Miranda, J. Phys. Chem. C, 2015, 119, 7386.
63. T. C. Anglin, D. B. O'Brien, A. M. Massari, J. Phys. Chem. C, 2010, 114, 17629.
64. T. C. Anglin, J. C. Speros, A. M. Massari, J. Phys. Chem. C, 2011, 115, 16027.
65. P. Dhar, P. P. Khlyabich, B. Burkhart, S. T. Roberts, S, Malyk, B. C. Thompson, A. V. Benderskii, J. Phys. Chem. C, 2013, 117, 15213.
66. T. C. Anglin, A. P. Lane, A. M. Massari, J. Mater. Chem. C, 2014, 2, 3390.
67. A. Morita, J. T. Hynes, Chem. Phys. 2000, 258, 371.
68. A. Morita, J. T. Hynes, J. Phys. Chem. B 2002, 106, 673.
69. B. Yurdumakan, G. P. Harp, M. Tsige, A. Dhinojwala, Langmuir, 2005, 21, 10316.
70. T. Ishiyama, A. Morita, J. Phys. Chem. C 2007, 111, 721.
71. H. Zhu, K. C. Jha, R. S. Bhatta, M. Tsige, A. Dhinojwala, Langmuir 2014, 30, 11609.
72. Y. Tong, Y. Zhao, N. Li, M. Osawa, P. B. Davies, S. Ye, J. Chem. Phys., 2010, 133, 034704.
73. D. B. O'Brien, A. M.Massari, J. Chem. Phys., 2013, 138, 154708.
74. M. Deighan, J. Pfaendtner, Langmuir, 2013, *29* (25), 7999.
75. A. P. Boughton, I. Andricioaei, Z. Chen, Langmuir, 2010, 26 (20), 16031.
76. W. Humphrey, A. Dalke, K. Schulten, J. Molecular Graphics, 1996, 14, 33.
77. D. A. Case, T. E. Cheatham, T. Darden, H. Gohlke, R. Luo, K. M. Merz, A. Onufriev, C. Simmerling, B. Wang, R. J. Woods, J. Comput. Chem., 2005, 26, 1668.
78. Y. Duan, C. Wu, S. Chowdhury, M. C. Lee, G. Xiong, W. Zhang, R. Yang, P. Cieplak, R. Luo, T. Lee, J. Caldwell, J. Wang, P. Kollman, J. Comput. Chem., 2003, 24, 1999.
79. J. Wang, R. M. Wolf, J. W. Caldwell, P. A. Kollman, D. A. Case, J. Computational Chemistry, 2004, 25, 1157.
80. C. Melis, L. Colombo, A. Mattoni, J. Phys. Chem. C 2011, 115, 576-581.
81. S. Obata, Y. Shimoi, Phys. Chem. Chem. Phys., 2013, 15, 9265.
82. C. Caddeo, A. Mattoni, Macromolecules, 2013, 46, 8003.
83. J. Li, T. Zhu, C. J. Cramer, D. G. Truhlar, J. Phys. Chem. A, 1998, 102, 1820.
84. W. L. Jorgensen, J. Chandrasekhar, J. D. Madura, R. W. Impey, and M. L. Klein, J. Chem. Phys., 1983, 79, 926.
85. J. C. Phillips, R. Braun, W. Wang, J. Gumbart, E. Tajkhorshid, E. Villa, C. Chipot, R. D. Skeel, L. Kalé, K. Schulten, J. Computational Chemistry, 2005, 26, 1781.
86. S. Ludwigs, Advances in Polymer Science, 2014, 265, Springer-Verlag Berlin Heidelberg.
87. L. H. Jimison, S. Himmelberger, D. T. Duong, J. Rivnay, M. F. Toney, A. Salleo, J. Polym. Sci., 2013, 51, 611.
88. M. C. Gurau, D. M. Delongchamp, B. M. Vogel, E. K. Lin, D. A. Fischer, S. Sambasivan, L. J. Richter, Langmuir, 2007, 23, 834.
89. X. T. Hao, T. Hosokai, N. Mitsuo, S. Kera, K. K. Okudaira, K. Mase, N. Ueno, J. Phys. Chem. B, 2007, 111, 10365.
90. W. D. Oosterbaan, J.-C. Bolsée, L. Wang , V. Vrindts, L. J. Lutsen, V. Lemaur, D. Beljonne , C. R. McNeill, L. Thomsen, J. V. Manca, D. J. M. Vanderzande, Adv. Funct. Mater., 2014, 24, 1994.
91. Q. Wei, S. Miyanishi, K. Tajima, and K. Hashimoto, ACS Appl. Mater. Interf., 2009, 1, 2660.
92. Q. Wei, K. Tajima, and K. Hashimoto, Appl. Phys. Lett., 2010, 96, 243301.
93. Y. D. Park, D. H. Kim, J. A. Lim, J. H. Cho, Y. Jang, W. H. Lee, J. H. Park, K. Cho, J. Phys. Chem. C, 2008, 112, 1705.
94. T. Kushida, T. Nagase, H. Naito, Appl. Phys. Lett., 2011, 98, 063304.
95. Y. Y. Yimer, A. Dhinojwala, M. Tsige, J. Chem. Phys., 2012, 137, 044703.
96. Y. Y. Yimer, M. Tsige, J. Chem. Phys., 2012, 137, 204701.
97. J. Ma, K. Hashimoto, T. Koganezawa, K. Tajima, J. Amer. Chem. Soc., 2013, 135, 9455.
98. J. Ma, K. Hashimoto, T. Koganezawa, K. Tajima, Chem. Commun., 2014, 50, 3627.
99. T. J. Prosa, M. J. Winokur, J. Moulton, P. Smith, A. J. Heeger, Macromolecules, 1992, 25, 4364.



 